CO2 from direct air capture as carbon feedstock for Fischer-Tropsch chemicals and fuels: Energy and economic analysis

Journal of CO2 Utilization 46 (2021) 101487

Contents lists available at ScienceDirect

Journal of CO2 Utilization

journal homepage: www.elsevier.com/locate/jcou

CO_2 from direct air capture as carbon feedstock for Fischer-Tropsch chemicals and fuels: Energy and economic analysis

Marco Marchese *[,1], Giulio Buffo [1], Massimo Santarelli, Andrea Lanzini

Department of Energy, Politecnico di Torino, Corso Duca degli Abruzzi 24, 10129 Torino, Italy

ARTICLE INFO

Keywords:
CO_2 utilization
Process integration
Direct air capture
Fischer-Tropsch
Techno-economic analysis
Hydrogen generation

ABSTRACT

The investigated plant concept integrates the direct air capture technology with the Fischer-Tropsch synthesis. 250 kt/h of air, with a CO_2 concentration of 400 ppm, are used as feedstock to produce the synthetic hydrocarbons. The direct air capture is modelled as a high-temperature calcium recovery loop process. An alkaline electrolyser and a reverse water-gas shift reactor produce the required syngas. The Fischer-Tropsch products distribution is described by a carbide model developed for a Co-Pt/γAl_2O_3 catalyst for alkanes and alkenes of carbon number C_1-C_{70}. Five integration scenarios are analysed. In the base case, the energy demand of the direct air capture process is supplied with natural gas from the distribution grid. In improved configurations, the effect of Fischer-Tropsch off-gas recirculation to the reverse water-gas shift and/or the direct air capture units is explored, excluding the need of fossil fuel. An electrified direct air capture solution is also included. In the analysed scenarios, the highest system efficiency corresponds to 36.3 %, while the maximum carbon dioxide conversion is of 68.3 %. The maximum waxes production corresponds to 8.7 t/h. Lastly, capital and operating plant costs are allocated in an economic investigation, considering different market electricity costs and financial risk values. In a medium financial risk scenario (interest rate: 7.5 %), the minimum Fischer-Tropsch waxes production cost corresponds to 6.3 €/kg_{wax}, reaching 5.05 €/kg_{wax} at an interest rate of 0%. Lastly, the effect of learning curves over the production cost at the year 2030 and 2050 is included.

1. Introduction

Solutions to reduce CO_2 emissions can involve different portfolios of mitigation measures: lowering energy and resource intensity, increasing the rate of decarbonization, and enhancing the reliance of carbon dioxide removal technologies [1]. In this framework, the European Union has pledged its commitment to achieving climate-neutrality by 2050 [2].

One way to reach such an achievement, is through the utilization of non-fossil carbon sources [3–5]. In non-fossil applications, hydrogen can be produced via electrochemical processes fed by electricity from renewable energy sources (RES). H_2 is then combined with a carbon feedstock to produce synthesis gas, determining the utilization of CO_2 available from a carbon capture process (namely, CCU). The resulting synthetic gas (i.e., syngas) is further upgraded to synthetic gaseous/liquid fuels and chemicals of practical use and market value [6]. In most of the analyzed scenarios forecasting future net-zero GHG emissions, CCU routes with thermo-/electrochemical processes are expected to play a vital role for the decarbonization of several economic sectors and the increased integration of RES in the electricity generation portfolio and manufacturing [2,6].

For these production chains, ambient air is attracting interest since it might be considered a nearly unlimited CO_2 resource available regardless of the plant location. Hence, research activity has been flourishing in recent years to exploit the carbon content of ambient air through Direct Air Capture (DAC) and reduce the atmospheric CO_2 concentration [7–9]. DAC through sorbent-based processes is studied to increase the removal rate ensured by the natural sinks in carbon cycles and enhance CO_2

Abbreviations: AF, Annuity factor; AFS, Anderson-Flory-Schultz; BEC, Bare erected cost; CAPEX, Capital cost; CC, Combined cycle; CCU, Carbon Capture and Utilization; CEPCI, Chemical Engineering Plant Cost Index; CSP, Concentrated solar power; DAC, Direct air capture; DCF, Discounted cash flow; FCF, Free cash flow; FT, Fischer-Tropsch; HX, Heat exchanger; KPI, Key performance indicators; LCA, Life cycle analysis; LHV, Lower Heating Value; NG, Natural gas; NPV, Net present value; O&M, Operation and maintenance; OG, Off-gas; OPEX, Operating cost; PtL, Power-to-liquid; PV, Photovoltaic; RES, Renewable energy source; RKS, Redlich-Kwong-Soave; RKS-BM, Redlich-Kwong-Soave, with Boston-Mathis modification; RWGS, Reverse water gas shift.

* Corresponding author.
E-mail address: marco.marchese@polito.it (M. Marchese).

[1] The authors equally contributed to the process model development.

https://doi.org/10.1016/j.jcou.2021.101487
Received 28 October 2020; Received in revised form 9 February 2021; Accepted 15 February 2021

Nomenclature

Esp_{CO2}	Specific energy consumption over the CO_2 removed from the air (kWh kg_{CO2}^{-1})
Esp_{wax}	Specific energy consumption over the waxes produced (kWh kg_{wax}^{-1})
i	Interest rate
k-year	k-th operational year
$\dot{m}$	Mass flow rate (kg h^{-1})
n	Scaling factor
$\dot{n}$	Molar flow rate (mol s^{-1})
n_{life}	Plant lifetime
Q_{th}	Thermal power (kW)
S_i	Size of the system component
W_{el}	Electric power (kW)
ΔH	Enthalpy change
η_C	Carbon conversion efficiency
η_{CO2}	Carbon dioxide removal efficiency
η_{GI}	Plant global efficiency

mitigation. For DAC applications, chemical sorbents are required to effectively capture CO_2, given its low concentration in ambient air [10]. Causticization with alkali and alkali-earth aqueous hydroxide sorbents [11], solid alkali carbonates [12] and organic-inorganic hybrid sorbents [10] are possible options to capture CO_2 from the air through reversible chemisorption.

The captured molecules can be used as raw material into carbon capture and utilization routes, producing several synthetic products [13], including Fischer-Tropsch (FT) material. CO_2 can be combined with H_2 or steam to form syngas via electrochemical or thermochemical catalytically driven processes [14]. Exothermic hydrogenation of CO to synthetic hydrocarbons inside the FT reactor is then applied [15]. The resulting products comprise of alkanes, alkenes and alcohols in gas, liquid, and wax phases. The advantage of the FT synthesis is the capability of targeting multiple hydrocarbons, with carbon numbers from C_1 to C_{100+} [16]. Specifically for high molecular weight products, the source is usually of fossil form. Therefore, the synthesis of long-chain FT hydrocarbons from CO_2 becomes strategic to reduce the consumption of fossil material not only in the transport sector but also in the chemical sector [17,18].

Much research effort has been spent in recent years in designing and demonstrating the integration of DAC into CCU routes. The Soletair project [19] and the Kopernikus Project [20] are examples of applications to synthesize FT products from air CO_2. Although these represent small-scale pilot applications, they are promising in establishing the effectiveness of this route. As reported in Table 1, most of the literature works on DAC-to-FT mainly deal with the life-cycle analysis (LCA) and the economic feasibility of the process, and the assessment of its role in current and future economic scenarios. For instance, Viebahn et al. [21] explored the possible role of the DAC into the German technology portfolio, through a multi-dimensional analysis to highlight the research needs that this technology still demands. The authors presented the best practices for DAC integration with several downstream technologies. However, their work was not focused on modeling, nor energy analysis. In the configuration of the FT route, they used exogenous productivity data from existing operating plants, without modeling information. van der Giesen et al. [22] investigated the LCA of solar liquid FT fuels production, comparing their environmental impact against their fossil counterparts. The FT reaction kinetics was not implemented in the study and the two sections of the scheme were not integrated into mass nor thermal terms. Fasihi et al. [23–25] investigated the production of FT fuels in a cost-optimized power-to-liquid routes, exploiting CO_2 from the air and a hybrid PV-wind power plant. The authors included a recirculation of the FT off-gas to produce electric energy in a combined cycle gas turbine to sustain the endothermicity of an electrified RWGS reactor. Contrarily to the present model, they employed a DAC section based on the solid sorbent technology and utilized clustered data for the FT products distribution taken from literature. Recently, Liu et al. [26] focused on the LCA of a high temperature DAC system paired with an FT unit to produce transportation fuel (i.e., diesel). The analysis was based on data and models from other works (e.g., Mansouri et al. [27] for the simplified FT synthesis power-law description and Keith et al. [28] process data for the DAC unit). Nonetheless, the authors highlighted the need for extensive DAC-FT matching analyses to maximize emissions reductions, as the focus of their study was not on the process integration.

In our work, we provide a detailed assessment on the techno-economic performance of a DAC-to-FT CCU plant. By means of process and energy integration, we identify the most suitable configuration to maximize CO_2 conversion into synthetic chemical and fuel feedstocks. Hence, the present work provides new and novel results on the DAC-to-FT route, filling the gap of system matching investigation. Firstly, the integrated DAC-to-FT process model is presented. Five separate configurations based on different FT off-gas recirculation solutions are studied, including detailed energy and mass integrations and the evaluation of key performance indicators (i.e., the specific energy consumption of carbon capture and conversion, carbon removal efficiency, system global efficiency). A solution with an electrified high temperature DAC section is also investigated. Secondly, a detailed mechanistic kinetic model describing the FT product distribution up to carbon number C_{70} is adopted. This allows identifying the plant design that synthesises the highest quantity of heavy hydrocarbons (i.e., wax fraction) while maximizing the CO_2 removal rate from the air and studying the effect of each plant configuration on the FT products distribution. Lastly, economic considerations are provided to estimate the cost of FT waxes production under each plant design. Sensitivities over the interest rate, the cost of electricity from different renewable energy sources and carbon credits solutions are provided. Additionally, learning curves estimation at the year 2030 and 2050 provide the evolution of the cost of production of FT waxes over the next decades with this route. Thus, this work represents a milestone in the development of highly integrated plants to produce synthetic FT material from the air, and represents the first investigation in terms of FT wax production costs from air CO_2.

2. Methods

The proposed system comprises of three main blocks: the capture of CO_2 from ambient air; the generation of syngas; the FT reaction for the synthesis of hydrocarbons. The process developed in this study is depicted in Fig. 1. The mass and energy balances of the different sections and the thermodynamic transformations of the operating streams were obtained using the commercial process simulator Aspen PLUS™. Large-scale data based on the DAC process proposed by Keith et al. [28] for the recovery of carbon dioxide from ambient air are used. The DAC system is connected to a reverse water-gas shift (RWGS) and an FT reactor. Moreover, in compliance with the model of Keith et al. [28], a natural gas (NG) turbine is used to meet the DAC section electric needs. NG is also fed to the DAC calciner reactor to meet its thermal needs. The process is studied under five plant designs, in terms of FT products synthesis and distribution, plant efficiency and carbon removal efficiency. The base process design considers NG supplied to the gas turbine and calciner, with FT off-gas recirculated to the RWGS (C.1). The upgraded configurations contemplate the avoidance of fossil natural gas, with recirculation of part of the FT off-gas to the DAC unit (configuration C.2), or to both the DAC and the RWGS (configuration C.3). Additionally, configurations C.4 and C.5 exclude the use of the power island, with C.4 having an electrified calciner, and C.5 utilizing the FT off-gas to the calciner. More details are found in section 2.4.

Table 1
Literature articles on DAC-FT processes and position of our research work compared to study objective, type of DAC and FT units, and application of recirculation of the FT off-gas.

Ref.	Study Objectives	DAC-section	FT-section	FT off-gas recirculation
[19]	Results of a pilot plant within the Finnish national project SOLETAIR	Low-T Hydrocell-based technology	Experimental distribution	Not included, suggested within the SOLETAIR Project
[29]	Assessment of combustion properties of FT fuels for aviation	Not modelled – mentioned among the CO_2 sources for the Kopernikus Project	Experimental distribution	FT off-gas recycle possibility to the RWGS - not modelled
[22]	LCA for Liquid FT fuels, using different carbon sources	Low-T, model after [30]	No kinetic model, Shell FT reactor data	Not included, off-gas assumed for steam generation and mild heat recovery from FT to RWGS catalyst regeneration. No integration to the DAC unit
[31]	LCA and economic assessment for FT jet fuels	Low-T Climeworks-based technology (no model, only energy consumption)	Not modelled. Only assumed 90 % syngas-to-hydrocarbon conversion	Not included nor discussed. Only water recycle
[32]	LCA and economic assessment for FT fuels in 2015/2030	Low-T Climeworks/Lackner et al. for CO_2 cost. Not modelled	Not modelled. Literature-based syngas-to-hydrocarbon conversion of 71 %	Not included
[33]	Assessment of combustion processes and emission of e-fuels (FT/OMEx) and LCA when using CO_2 from DAC	N.A.-not modelled	N.A. Evaluation of fuels from tanks	Included only as exhaust gas recirculation - not intended as FT production yield increment
[26]	LCA for liquid FT transportation fuels w/ sensitivity on the carbon intensity of electricity source	High-T C.E.-based technology and model	Simple power-law kinetic model [27]. No FT products full distribution description	Not included, off-gas assumed for steam generation and CHP. Only sensitivity on the H_2/CO and FT temperature. No detailed information on the FT products distribution
[34, 35]	Review, Environmental and Techno-Economic assessment of PtL routes (MeOH/FT)	Low-T, Climeworks-based technology	FT process based on literature data. Not modelled	Not included
[21]	Best practices for DAC integration into the German's technology horizon	Multiple technologies accounted	Productivity data from operating plants/pilot plants. Not modelled	Not included. Detailed integrated energy model not a study goal
[36]	Review article of the CO_2 conversion through FT	–	–	Mentioned within SOLETAIR Project description but not discussed
[37]	Review of CO_2 recycling pathways, techno-economic analysis for the production of synthetic fuels from CO_2 captured from the air and solid oxide co-electrolysis to Fischer-Tropsch.	Solid sorbent DAC at low-T operations (45 °C). Black box with energy consumption and CO_2 stream cost	State-of-the-art High Temperature Fischer-Tropsch technology (300 °C), not modelled with detailed products distribution	Recovery of heat from the Fischer-Tropsch reactor. No information provided over FT off-gas recirculation
[23,24, 25, 38, 39]	TEA forecast scenarios for transportation fuels production (including FT-derived fuels) based on cost-optimized renewable power plants and capture of CO_2 from the air technologies.	Low-T DAC unit accounting for energy and costs related to the Climeworks technology	Low-Temperature Fischer-Tropsch unit with mass share of clustered products based on literature data.	Account for heat and mass integration. Recirculation of the FT off-gases is studied towards a combined cycle gas turbine to sustain an electrified RWGS
[25]	Report on the cost of liquid fuels based on the MeOH and FT technologies utilizing CO_2 from the air in the country of Germany	Description and energy/ economic data based on Climeworks low-T configuration	Fischer-Tropsch description based on literature data [24,25].	Not mentioned, but most likely accounted as off-gas recirculation for electric generation based on literature studies [24, 25].
[40]	Description of the Direct Air Capture technology as a key technology to produce carbon-based materials (minerals and fuels)	Low-T technology based on Climeworks application	Not described, only mentioned for transportation fuels productions.	Not included
[41]	Production of FT syncrude based on either biomass gasification or DAC fed with intermittent RES coupled with CO_2 storage unit	Modelling of the DAC not provided	Fischer-Tropsch model based on experimental data on a commercial catalyst [42]	Not included
[43]	Techno-economic assessment with forecast scenarios of kerosene production in Germany, exploiting CO_2 from air, biomass, and CO_2 from flue gases as carbon feedstocks	Both the DAC and the FT performance and cost data are taken from literature works. No information about modelling, mass and energy integration, nor recirculation if provided.		
[44]	Review of PtL technologies (reactors and materials, production costs) for the production of MeOH, DME, and FT fuels from air CO_2 capture with DAC technology	Description of DAC technologies and their applications in PtL routes	Description of FT reactors and products share	Not included
[45]	Evaluation of production cost of synthetic liquid hydrocarbons based on different CO_2 sources (industry, air, biomass), most profitable production chains, and allocation of end-products	Literature data based on unspecified DAC cost configuration projected to the year 2050	Literature data [34]	–
This study	DAC + FT energy and mass integration for enhanced wax production yield and economic evaluation. Effect of process configuration on the FT products distribution	High-T C.E.-based technology and model	Detailed mechanistic kinetic model, describing the full FT products distribution	In-depth analysis to evaluate the best recirculation design of the FT gas fraction for enhanced wax production and CO_2 mitigation potential

2.1. Direct air capture

The process of DAC was modelled taking the cue from a reference layout based on calcium recovery loop, similar to the work proposed by Keith et al. [28]. The process chemistry is described by the following reactions:

In the DAC section, two separate loops are identified: the first one comprising of an air contactor, an absorber column, and a pellet reactor for CO_2 capture; the second one involving the pellet reactor, a cyclone, a washer, a slaker and a calciner reactor. In the air contactor, CO_2 (400 ppm in air) was removed from ambient air through an aqueous alkali solution of 1.0 mol OH^-, 0.5 mol CO_3^{2-} and 2.0 mol K^+ yielding $K_2CO_{3(aq)}$. The capture rate of this component was set to 75 % of CO_2 in the form of $K_2CO_{3(aq)}$ [28]. Similarly, 90 % of the CO_2 contained in the

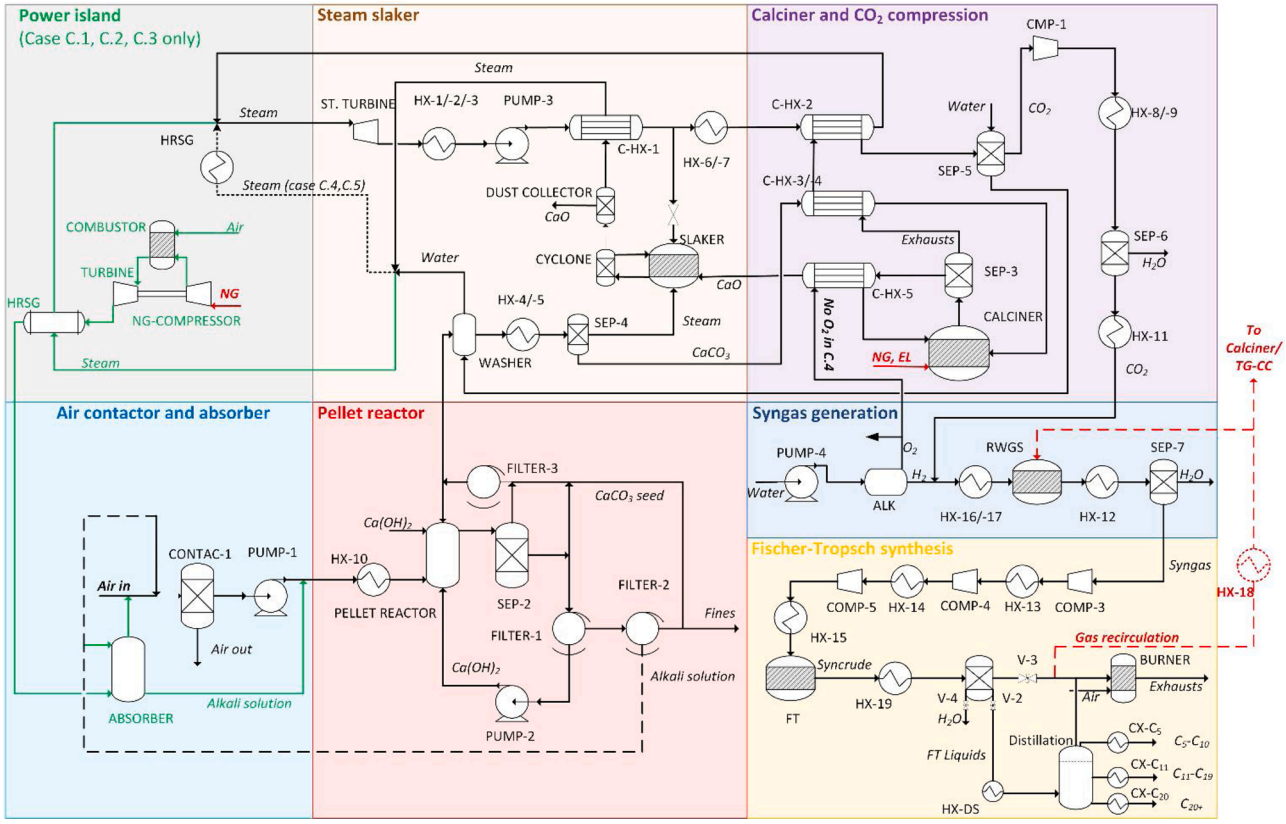

Fig. 1. Proposed DAC-FT system. Only the baseline configuration (C.1) presents natural gas fed to the DAC. For configurations C.1, C.2, and C.3 there exists a power island (highlighted with green solid lines and text), which is excluded in configurations C.4 and C.5.

exhausts leaving the combined cycle was absorbed in a packed column (absorber). The stripped-off gas was mixed with ambient air. The calcium loop regenerated the alkali capture solution through the precipitation of CO_3^{2-} reacting with Ca^{2+} of $Ca(OH)_2$ in the pellet reactor, forming $CaCO_3$ via reactions 5−6 (Table 2). This pellet reactor was simulated with a crystallizer reactor component of Aspen PLUS™ implementing reactions 5–10, ensuring calcium retention equal to 90 % (i.e., the share of injected calcium leaving the reactor as pellets rather than being disposed of as fines) [28]. The precipitation of calcium carbonate pellets is adapted from a fluidized-bed crystallizer commercialized by RHDHV [46] used also for DAC applications. The $CaCO_3$ pellets were washed, dried, heated up and entered an oxygen-fired calciner (95.6 % O_2, 4.4 N_2) with a $CaCO_3$-to-CaO conversion efficiency equal to 98 %. Finally, the concentrated stream of CO_2 leaving the calciner was washed in a water knockout and fed to the RWGS reactor. The complete combustion of NG in the calciner thermally sustained the endothermic decomposition of $CaCO_3$ pellets, thus providing adiabatic operations in the calciner. The stoichiometric reactor for the CaO hydration in the steam slaker was fed by a fraction of the steam in the bottom cycle of the combined cycle. A primary cyclone elutriated and recirculated small CaO particles to the slaker. The further CaO particles collected in the downstream dust collector can be disposed of or reused: their end of life is out of the scope of this study, but suggested to assess the potential savings of raw material and energy. The output $Ca(OH)_{2(aq)}$ was then fed to the pellet bed to react with K_2CO_3. Table S.1 in supporting material reports the specifications of the DAC main blocks.

Table 2
DAC unit chemical reactions.

Reaction	Type	Reaction	Type
1) $H_2O+HCO_3^- \leftrightarrow CO_3^{2-}+H_3O^+$	Equilibrium	6) $K_2CO_{3(S)} \leftrightarrow CO_3^{2-} +2\ K^+$	Salt precip.
2) $CaOH^+ \leftrightarrow Ca^{2+} +OH^-$	Equilibrium	7) $CaCO_3 \leftrightarrow CO_3^{2-} +Ca^{2+}$	Salt precip.
3) $2H_2O + CO_2 \leftrightarrow HCO_3^- +H_3O^+$	Equilibrium	8) $KOH_{(S)} \leftrightarrow OH^- +K^+$	Salt precip.
4) $2H_2O \leftrightarrow OH^- +H_3O^+$	Equilibrium	9) $K_2CO_3 \rightarrow CO3^{2-} +2\ K^+$	Dissociation
5) $Ca(OH)_2 \leftrightarrow CaOH^+ +OH^-$	Salt precip.	10) $KOH \rightarrow OH^- +K^+$	Dissociation

The properties and thermodynamic parameters of the chemical components were estimated with the unsymmetrical electrolyte non-random two-liquid method (for the liquid phase), Redlich-Kwong equation and Henry's Law for gas phase and Vapor-Liquid Equilibrium. In two-phase blocks, the mass transfer was modelled with a "two-film" rate-based approach neglecting the mixing by convection [47,48].

2.2. Syngas generation

The syngas, a mixture of H_2, CO, CO_2, and H_2O, was yielded at the RWGS reactor outlet and compressed to the operating pressure of the FT reactor.

2.2.1. Hydrogen generation

The required hydrogen was obtained through electrolysis of water in a low-temperature alkaline electrolyser. The electrolyser operated at ambient pressure and 60 °C and consumed 15 L_{H2O}/kg_{H2} and 52 kWh_{el}/kg_{H2} [49], resulting in a absorbed power ranging between 646 and 858 MW_{el}. The electric input to run the electrolysis process was assumed to be of renewable energy source (e.g., hydro, PV, wind, etc.), hence not affecting the carbon balance with indirect emissions associated to power generation. Balancing renewable energy production mismatch with the electrolysis power demand through a dynamic charging/discharging schedule of hydrogen storage is out of the scope of this work. Oxygen was considered as an electrolyser by-product, and a fraction of it was fed

to the calciner reactor to sustain the process of oxy-combustion and ensure adiabatic operation.

2.2.2. Reverse water-gas shift

CO_2 coming from the DAC unit was mixed with H_2 and preheated to 550 °C before entering the RWGS reactor operating at ambient pressure and 800 °C. The generated syngas had the desired H_2/CO outlet molar ratio of 2.0. The RWGS operated at equilibrium conditions, employing a Ni-Al_2O_3 catalyst [50], and described with Redlich-Kwong-Soave (RKS) equation of state. The conversion of CO_2-to-CO followed reaction 11 of Table 3, determining the high endothermicity of the reactor. In parallel, side reactions of methanation (12–13), Boudouard reactions (14–15), hydrocarbon cracking (16–17) were considered.

2.3. Fischer-Tropsch

A low-temperature FT reactor was operated at 230 °C and 25 bar. It converted the feed of syngas into synthetic hydrocarbons via catalytically driven reactions of CO with H_2. The syngas was compressed to the operating pressure before the FT reactor. A mechanistic carbide kinetic model for a Co-Pt/ɣAl_2O_3 catalyst was used to describe the production rate of the FT reactor [51]. The kinetic model was inserted in the process simulator via an external subroutine. The simplified chemical reactions are presented in Table 4. Thanks to the application of detailed kinetic model, each product generation rate and reactant consumption rate were accounted for. The distribution of the FT products followed a modification of the Anderson-Flory-Schultz (AFS) distribution, where a higher CH_4 generation, a lower C_2H_4 generation and a linearization of the curve for carbon numbers higher than C_{20} were obtained with respect to the AFS theory. A per-pass CO conversion of 75 % was assumed [52]. The products leaving this reactor comprised unreacted CO_2, CO and H_2, steam and alkanes and alkenes synthesised up to carbon number C_{70} and carbon number C_{40}, respectively. A three-phase (liquid-liquid-gas) separator operating at the FT pressure and ambient temperature separated the FT off-gas (CO, H_2, CO_2 and mainly light hydrocarbons up to carbon number $C_{6\text{-}7}$), the liquid products and water. The liquid products were preheated to 230 °C and further separated into a distillation column based on their boiling temperatures as naphtha (120 °C, C_5-C_{11}), middle distillates (225 °C, C_{11}-C_{20}) and waxes (380 °C, C_{20}-C_{70}). The liquid products were used to account for the energy performance of the full plant. The FT reactor used the RKS equation of state, with Boston-Mathis alpha-value modification. More details can be found at [52].

2.4. Plant upgrading and thermal integration

The recirculation of the FT off-gas can provide a variation in plant productivity and efficiency [53]. Additionally, they can be used as a solution to avoid feeding fossil natural gas to the system. Therefore, four additional plant designs were studied in this analysis. These configurations are presented in Fig. 2.

- Configuration C.1: the FT off-gas were recirculated at the RWGS reactor inlet. The recirculated stream included unreacted CO_2, H_2, CO and CH_4, and other light hydrocarbons in a lower concentration. These underwent steam reforming according to reaction 17, increasing the yield of syngas production. NG was fed to the DAC section, in accordance with the DAC configuration proposed by Keith et al. [28].
- Configuration C.2: the FT off-gas were recirculated to the DAC, substituting the NG stream. CH_4 and light hydrocarbons underwent oxy-combustion inside the calciner reactor and combustion inside the combined cycle. The fraction of off-gas recirculated to the combined cycle allowed covering the electric needs of the DAC system, while the remaining flow ensured adiabatic operations of the calciner reactor.
- Configuration C.3: the FT off-gas were recirculated to the RWGS reactor inlet and DAC unit. The off-gas recirculated to the DAC unit were distributed to both the combined cycle and calciner with the same criterion as in configuration C.2.
- Configuration C.4: the FT off-gas is recirculated to the inlet of the RWGS reactor. The combined cycled and the absorption column are excluded from the DAC section, and the calciner is electrically heated.
- Configuration C.5: even in this case the combined cycle and the absorption column are excluded from the model, and the calciner heat is provided by partial recirculation of the FT off-gas. The remaining part of the FT off-gas is fed to the RWGS reactor.

Table 3
RWGS reactor chemical reactions.

Reaction	ΔH^0_{298K}[kJ/mol]	Reaction	ΔH^0_{298K}[kJ/mol]
11) $CO_2+H_2 \leftrightarrow CO+H_2O_{(v)}$	+41	15) $2\,CO+H_2 \leftrightarrow H_2O_{(v)}+C_{(s)}$	−131
12) $CO+3H_2 \leftrightarrow CH_4+H_2O_{(v)}$	−165	16) $C_nH_m \leftrightarrow nC+(m/2)H_2$	e.g. + 791 CH_4
13) $CO_2+4H_2 \leftrightarrow CH_4+2H_2O_{(v)}$	−206	17) $C_nH_m+nH_2O_{(v)} \leftrightarrow nCO+(n+m/2)H_2$	e.g. + 206 CH_4
14) $2CO \leftrightarrow CO_2+C_{(s)}$	−172		

Table 4
FT reactor chemical reactions.

Reaction	ΔH^0_{298K}[kJ/mol]
18) $CO+2H_2 \leftrightarrow$ -(CH_2)-$+H_2O$	−165
19) $nCO+(2n+1)H_2 \leftrightarrow C_nH_{2n+2}+nH_2O$	Paraffins
20) $nCO+(2n)H_2 \leftrightarrow C_nH_{2n}+nH_2O$	Olefins

Under all configurations, a fixed electric output of 30 MWel from the combined cycle turbine was assumed. Moreover, the airflow to the combined cycle compressor for case C.1, C.2, and C.3 was iteratively changed to reach an absorber column inlet temperature of 93 °C [28].

Concerning the possible issue of resource availability, the process uses natural gas in C.1, for which it may not be installed anywhere; thus, our study assessed four designs (C.2 to C.5) that do not require any feed of natural gas to the calciner nor the combined cycle in the DAC section. These configurations are completely decoupled from the natural gas infrastructure, hence without any restriction about the installation site from this standpoint. Additionally, they allow having a solution where the only carbon source is the air. Concerning water consumption, this cannot be avoided since water is the essential feed stream for hydrogen production through electrolysis and is also used in the knockout section. Hence, it is worth remarking that water availability is extremely important when assessing the techno-economic feasibility of this technology and its integration in local contexts.

In any recirculation solution, a minimum value of 5% of the FT off-gas was fed to the burner at the FT separation unit outlet, avoiding the accumulation of inert gases in the plant lines [54]. The off-gas percentage sent to the RWGS in configurations C.3 and C.5 was evaluated accordingly:

$$OG\%_{RWGS} = 95\% - (OG\%_{C.Cycle} + OG\%_{Calciner}) \quad (1)$$

With the value to the combined cycle equal zero in C.5. NG had a composition of $CH_4/C_2H_6/CO_2/N_2$: 89/4/3/4mol-%. Finally, endothermicity and exothermicity of the different plant components were exploited to reduce the total plant thermal needs. The pinch analysis methodology was applied, identifying the optimal energy integration of the whole plant under each configuration.

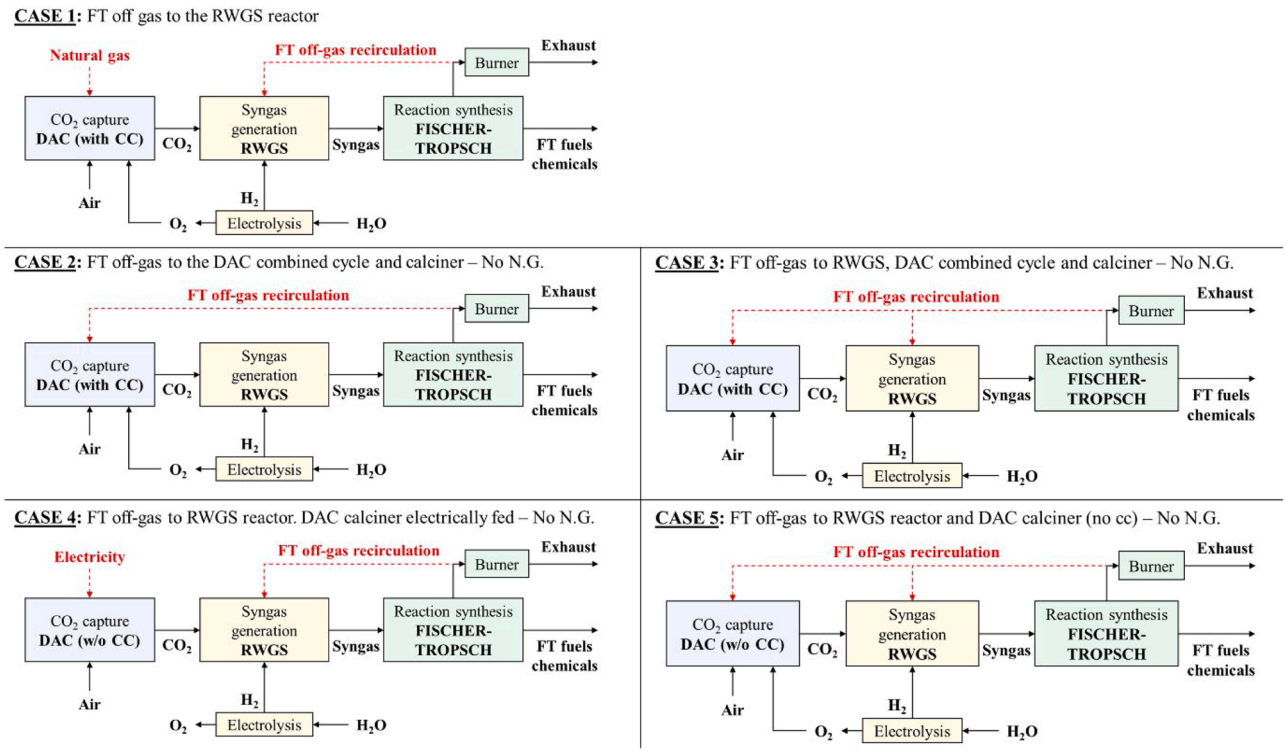

Fig. 2. Configurations studied in this work. Recirculation options are highlighted with red-dashed lines.

2.5. Economic assessment

To complete the investigation, an economic assessment was included. Starting from the mass and energy balances, the capital cost (CAPEX) and the annual operating costs (OPEX) of each system were computed, assuming:

- 8,000 operating hours per year;
- plant lifetime of 25 years;
- 2019 as the year for cost estimations (Chemical Engineering Plant Cost Index, CEPCI: 619 [55]);
- Costs in euros, at an exchange rate \$/€ of 1.145 when applied;
- no remuneration of invested capital;
- nor depreciation nor taxes, to be as more site-independent as possible.

The investment cost of the system was computed starting from exogenous data found in literature, adopting a top-down approach:

- for the DAC subsystem, a unit capital cost of 733 €/t_{CO2} y was assumed, actualizing the value provided by Fasihi et al. [9] for the installation of the N-th DAC plant and referred to an estimate by Carbon Engineering [56], including direct field costs, non-field costs and indirect costs. For the electrified configuration C.4 and configuration C.5 without combined cycle a cost of 562 €/t_{CO2} y and 549 €/t_{CO2} y for the N-th DAC installed unit was assumed, respectively [9].
- The bare erected cost (BEC) of the heat exchanger was assessed as a function of their power (S, in kW) [57]:

$$BEC_{HX} = 1.3 \cdot 144 \left(\frac{S}{150}\right)^{0.78} \quad (2)$$

where 144 k€ (2019, i.e., 130 k€ in 2015) is the bare module cost of a 150-kW heat exchanger and 1.3 is the installation factor. Indirect costs were assessed as half of the bare module cost [57]. This cost function is in good agreement with the one provided by Atsonios et al. [58] for large-size heat exchangers.

- For an alkaline electrolyzer (including the stack, power converters, water purification system, gas purification unit and water recirculation pump) with a nominal size equal to P_{WE} (kW), the following function fitting the data reported in [59] was derived:

$$\widetilde{c}_{BM,\,WE}\left[\frac{€}{kW}\right] = 1437 \cdot P_{WE}^{-0.095} \quad (3)$$

- The RWGS, the syngas compressors, the burner and the distillation column costs were evaluated utilizing eq. 4, as follows:

$$C_i = C_{ref,\,i}\left(\frac{S_i}{S_{ref,i}}\right)^{n}\left(\frac{CEPCI_{2019}}{CEPCI_{ref,i}}\right) \quad (4)$$

Being S and S_{ref} the model and reference size of the i-th component according to Table 5, C and C_{ref} the capital cost of the i-th component.

- Decker et al. [63] provided a linear cost function for the FT system, with a specific capital cost of 530 €/kW and an installation factor equal to 2.

The sum of the capital costs after contingencies and installation factors of the different sections represented the plant CAPEX, assuming a confidence range of the investment costs as ± 30 % [64].

Table 5
Cost parameters used for the RWGS, syngas compression, FT products distillation column and burner.

Element	n	S_{ref}	C_{ref}	Ref.
Burner	0.80	20.00 MW	1.97 M€	[60]
Syngas Compressor	0.68	0.413 MW	0.49 M€	[60]
Distillation Column	0.70	6.590 t/h	0.73 M$	[61]
RWGS	0.65	43.00 t/h	32.0 M$	[62]

The operating costs of the system were allocated to the different sections according to Table 6, which included electrical and non-electrical related costs derived from the systems operations. Catalysts replacements in the reactors were assumed every 3 years of operations [64].

For the electrolyser replacement, we have assumed its substitution every 10 years, with a direct dependency over the capacity of the device, according to the following equation [66]:

$$Alk_{Repl.}\left[\frac{€}{kw}\right] = \frac{2}{3}0.4\ Alk_{Capex} \quad (5)$$

Moreover, the sensitivity of the power-related OPEX (i.e., sensitivity over the electric costs) to the market price of electric energy from different renewable sources was assessed, considering the global-weighted costs valid in 2019 and taken from [68]:

- 41.05 €/MWh hydropower;
- 46.29 €/MWh – onshore wind;
- 59.39 €/MWh – PV;
- 63.76 €/MWh – geothermal;
- 100.44 €/MWh – offshore wind;
- 158.95 €/MWh – CSP (concentrated solar power).
- 210.00 €/MWh – Baseload electricity from hybrid PV-wind power plant [69].

Among the selected sources, hydropower can be considered the cheapest solution, but also constrained to resource availability throughout the year. Additionally, such a resource might be used for direct power demands, rather than being utilized in CCU routes. However, studies assessing the production of synthetic fuels and hydrogen with hydropower are available from the open literature [70,71], with the possibility of also matching power production and demand [72]. Moreover, the use of direct renewable energy might be non-trivial and affected by fluctuation and location, with the need of expensive hydrogen storage solutions at 470 €/kg_{H2} [49] (e.g., in PV or wind applications). Hence, baseload operations were also considered, as high capacity CCU plants for synthetic hydrocarbons can be connected to the electric grid supposing a feed of mixed renewable energy sources [69]. Adopting such a solution, might not represent cost-optimized values, depending on the site of installation.

The systems revenues were derived considering the sale of residual oxygen from the steam electrolysis not consumed internally to the system (sale value €/kg_{O2} 0.15 [73,74]) and the FT products of carbon number C_5-C_{20} separated from the resulted heavy wax fraction (i.e., naphtha at 0.31 $/l and middle distillates at 0.5 $/l [67]).

The discounted cash flow analysis [75] was performed considering three values of the interest rate to account for different levels of investment risks (i = 0% - low risk; i = 7.5 % - medium risk; i = 12.5 % - high risk), assuming total capital expenditure at year 0 [56]. The cash flow at the k^{th} year consists of the sum of the operating costs:

- Free Cash Flow:

$$FCF_k = OPEX_k - Revenue_k \quad (6)$$

- Discounted Cash Flow:

$$DCF_k = \frac{FCF_k}{(1+i)^k} \quad (7)$$

- Net present value, i.e. the total money flow during the plant lifetime (n_{life}):

$$NPV = CAPEX + \sum_{k=1}^{n_{life}} DCF_k \quad (8)$$

Lastly, at each interest rate value, the cost of Fischer-Tropsch waxes production was assessed [€/kg_{wax}], considering as lower and upper boundaries the electricity generation costs of hydropower and CSP sources, respectively:

$$\text{Wax cost} = \frac{NPV}{\dot{m}_{wax_{out}} \cdot AF} \quad (9)$$

where $\dot{m}_{wax,out,}$ is the wax mass flow rate. AF is the annuity factor computed as:

$$AF = \frac{1-(1+i)^{-n_{life}}}{i} = \sum_{k=1}^{n_{life}} \frac{1}{(1+i)^k} \quad (10)$$

2.5.1. Future production costs

In the case of baseload electricity, the cost of producing FT waxes was assessed with reference to the year 2030 and 2050 by application of learning curves for the involved technologies and reduction in the baseload power cost. 15 % learning rate was assumed for the DAC unit, as reported in [9]. The cost of alkaline was reduced over time to 415 €/kW and 220 €/kW in 2030 and 2050, as listed by Gorre et al. [76]. Finally, 10 % learning rate was included for the installation of 100 units for the RWGS and FT, in accordance with the statements available from [77] and [78]. The baseload electricity cost corresponded to 75 €/MWh and 60 €/MWh in 2030 and 2050, respectively [69].

2.6. Key performance indicators

Key performance indicators (KPIs) were evaluated for each plant solution. The specific plant energy consumption was estimated and expressed both in terms of CO_2 removed from the air and FT waxes production, and expressed as kWh/kg_{CO2} and kWh/kg_{wax}, respectively:

$$E_{SP_{CO_2}} = \frac{W_{el_{in}} + Q_{th_{in}} + \dot{n}_{NG} \cdot LHV_{NG}}{\dot{m}_{Co_{2_{rem}}}} \quad (11)$$

$$E_{SP_{wax}} = \frac{W_{el_{in}} + Q_{th_{in}} + \dot{n}_{NG} \cdot LHV_{NG}}{\dot{m}_{wax_{out}}} \quad (12)$$

$$\dot{m}_{Co_{2_{rem}}} = \left(\dot{m}_{CO_{2_{AIR_{in}}}}\right) - \left(\dot{m}_{CO_{2_{AIR_{out}}}} + \dot{m}_{CO_{2_{EXH_{out}}}}\right) \quad (13)$$

where $\dot{m}_{CO2,air,in}$, $\dot{m}_{CO2,air,out}$ and $\dot{m}_{CO2,exh,out}$ are the mass flow rate of CO_2 in the streams denoted as "Air in", "Air out" and "Exhaust" in Fig. 1. The $W_{el,in}$ and $Q_{th,in}$ terms represent the net electrical and thermal power required by the plant (kW), respectively. $\dot{n}_{NG}$ is the molar flow rate of NG (mol/s). LHV is the lower heating value of NG (kJ/mol).

The carbon efficiency (η_C) was also evaluated. This parameter

Table 6
Operating costs of the different sections of the system. [a]Reference to the section CAPEX. [b]Includes syngas compression, products distillation, and off-gas combustor.

OPEX	Value	Ref.	DAC	Alk	HEN	RWGS	FT[b]
Non-electric costs							
O&M (% CAPEX[a])	3.70 3.00	[9] [60,61,62,65]	X	X	X	X	X
Water consumption (€/m^3)	0.09	[56]	X	X	X		
Alk. repl. every 10 years (k€/kW)	Eq. (5)	[66]		X			
Cat. repl. every 3 years (%)	1.00	[64]				X	
Cat. repl. every 3 years (€/kg)	112.9	[67]					X
NG to CC/calciner (€/MWh)	11.3	[56]	X				
Electric costs	–		X	X	X		X

accounted for the carbon that is converted into FT liquid products in all the considered configurations.

$$\eta_C = \frac{\left[\left(\dot{n}_{C_{AIR_{in}}} + \dot{n}_{C_{NG_{in}}}\right) - \left(\dot{n}_{C_{AIR_{out}}} + \dot{n}_{C_{EXH_{out}}}\right)\right]}{\dot{n}_{C_{AIR_{in}}} + \dot{n}_{C_{NG_{in}}}} \quad (14)$$

$\dot{n}_{C,AIR,in}$ and $\dot{n}_{C,NG,in}$ are the molar flow rates of carbon entering the system with "Air in" flow rate and the NG stream, respectively. $\dot{n}_{C,AIR,out}$ and $\dot{n}_{C,EXH,out}$ are the molar flow rates of carbon leaving the system with "Air out" flow rate and the exhausts of the burner after the FT, respectively.

The efficiency of carbon dioxide removal from the air (η_{CO2}) was evaluated according to the following formula:

$$\eta_{CO_2} = \frac{\left[\left(\dot{n}_{CO_{2_{AIR_{in}}}}\right) - \left(\dot{n}_{CO_{2_{AIR_{out}}}} + \dot{n}_{CO_{2_{EXH_{out}}}}\right)\right]}{\dot{n}_{CO_{2_{AIR_{in}}}}} \quad (15)$$

$\dot{n}_{CO2,AIR,in}$ is the molar flow rate of carbon entering the system with "Air in" stream. $\dot{n}_{CO2,AIR,out}$ and $\dot{n}_{CO2,EXH,out}$ are the molar flow rates of carbon leaving the system, respectively, with the "Air out" flow rate and the exhausts of the burner.

The total plant efficiency (η_{GI}) was computed as the ratio of the chemical power of the FT liquid products to the plant consumption of electricity (including electrolysis demand), external heat and NG supply (where *LHV* stands for lower heating value) as follows:

$$\eta_{GI} = \frac{\sum \dot{n}_{FT_{liq}} \cdot LHV_{FT_{liq}}}{W_{el_{in}} + Q_{th_{in}} + \dot{n}_{NG} \cdot LHV_{NG}} \quad (16)$$

In Eqs. ((13)–(15)), the terms referring to NG stream existed only for configuration C.1.

3. Results and discussion

3.1. Mass balances of analysed configurations

The results regarding the mass balances are summarized in Table 7. Concerning the DAC section, all configurations process 250,000 t/h of air, containing 150 t/h of carbon dioxide. This flow joins the gas coming from the absorber, where CO_2 is captured from the exhausts of the combined cycle for C.1, C.2 and C.3. Apart from the baseline configuration C.1, the only source of carbon material is the ambient air stream entering the system. Contrarywise, in configuration C.1 the sources of carbon material are ambient air and NG. The latter injects an additional stream with 14.5 t/h of C into the plant.

Regarding the FT synthesis section, configuration C.1 provides 207.3 t/h of gas fraction and 33.6 t/h of the liquid fraction. The products distribution is presented in Fig. 3. In the same figure, the distribution is broken down into its main contributors: the figure highlights the difference between the gas fraction, separated in the liquid-liquid-gas separator at the outlet of the FT reactor, and the olefins and paraffins in the liquid fraction. The gas fraction is mainly composed of methane, which also accounts for 38.6 %-mol of the total FT products, with a lower concentration of light hydrocarbons up to carbon number C_4. Considering the liquid fraction, paraffins represent the most relevant compound contributors, with a peak around carbon number $C_{7\text{-}8}$, while the olefins can be considered relevant in the carbon number range $C_{2\text{-}12}$, with a peak around $C_{6\text{-}7}$. This is in good agreement with the research in the field of cobalt-based FT synthesis, where the paraffin fraction is increasingly more influent over the olefins at increasing carbon numbers [79]. It is to note that the total distribution follows the modification of the AFS theory for FT products, as predicted by the kinetic model, and it reaches a linearization of the curve for carbon number higher than $C_{18\text{-}20}$. However, compared to the traditional FT distribution, there exists a shift towards heavier hydrocarbons, due to the recirculation of the FT off-gases, providing a local peak at C_7 (a direct comparison of the FT distribution with and without recirculation is available in the Supporting Material).

Table 7
Mass balance information.

Mass flow rate [t/h]	*C.1*	*C.2*	*C.3*	*C.4*	*C.5*
Air inlet	250000.0	250000.0	250000.0	250000.0	250000.0
Air outlet	248354	248379.7	248377.9	248163.1	248163.1
C. Cycle Exhausts	232.5	244.1	242.9	0.0	0.0
Absorber Solvent	347.0	290.2	287.3	0.0	0.0
Air Contactor Solvent	2767.7	2764.2	2761.7	2681.6	2681.6
H_2O Knockout	531.0	531.0	531.0	531.0	531.0
Natural Gas to C. Cycle	12.2	–	–	0.0	0.0
Natural Gas to Calciner	110.1	–	–	0.0	0.0
Air to C. Cycle	220.3	223.1	223.6	0.0	0.0
Air to Burner	222.4	189.1	92.2	146.9	140.4
Burner Exhausts	233.8	207.7	98.7	152.7	148.7
Condensed H_2O	130.9	75.1	84.1	74.5	94.3
CO_2 to RWGS section	123.9	159.9	149.7	93.9	142.4
H_2O electrolysis	250.5	211.3	234.4	193.3	256.5
O_2 electrolysis	133.5	113.1	124.9	103.4	137.2
to Calciner	*29.5 %*	*33.7 %*	*29.8 %*	–	*25.5 %*
FT Products	240.9	99.0	117.3	114.5	163.2
Gas fraction to burner	*11.4*	*18.4*	*6.5*	*5.8*	*8.3*
Gas fraction recirculated	*195.9*	*67.4*	*92.3*	*82.1*	*128.6*
Liquid/Wax fraction					
(C_5-C_{11})	*11.98*	*5.01*	*6.98*	*9.94*	*9.75*
(C_{11}-C_{20})	*12.9*	*4.7*	*6.63*	*9.72*	*9.66*
(C_{20+})	*8.7*	*3.5*	*4.8*	*6.94*	*6.83*
Gas fraction recirculation					
to RWGS	*95.0 %*	–	*37.1 %*	*95.00 %*	*77.30 %*
to C. Cycle	–	*24.9 %*	*19.9 %*	–	–
to Calciner	–	*54.7 %*	*38.0 %*	–	*22.70 %*

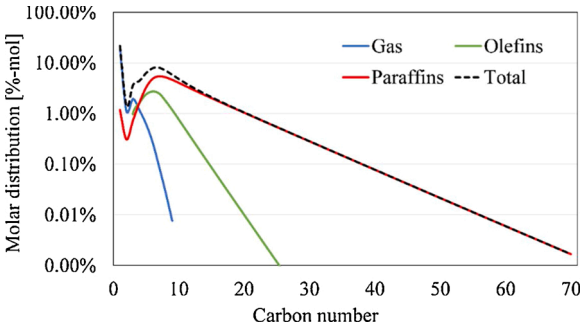

Fig. 3. FT products distribution of C.1: global FT distribution (black dashed line) and break-down of the products' components.

Depending on the recirculation solution applied (to the RWGS and/or the DAC) the throughput of synthetic material collected at the outlet of the FT reactor changes, and so does the FT distribution. Such a trend can be noticed from the results listed in Table 7 and from the FT distributions provided in Fig. 4. With respect to the production of FT material, configurations C.2 to C.5 all present a slight reduction in the total amount of FT hydrocarbons with respect to the baseline C.1: the difference is particularly significant for products with a carbon number higher than C_4 (C_5 for configuration C.2). Configuration C.1 seems to be the most suitable solution when targeting a high amount of FT liquid products. This behavior could be linked to different factors. Firstly, C.1 introduces in the system more carbon with the NG flow, determining a higher amount of carbon material looping in the plant that reacts to

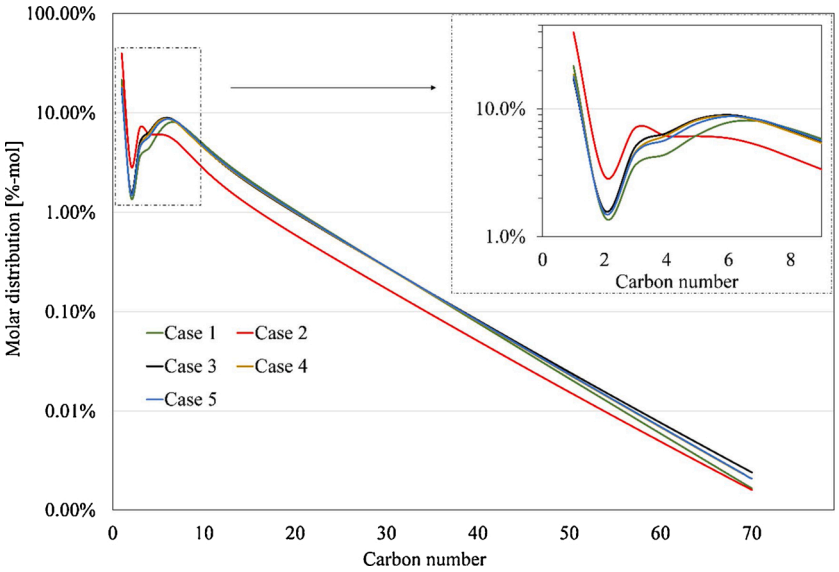

Fig. 4. FT products distribution: scenarios comparison on molar share.

synthetic FT compounds. Secondly, C.2 and C.3 deliver a part of the carbon dioxide entering the system back to the air contactor, whose capture efficiency of 75 % determines a small loss of carbon material towards the environment [28]. This could also explain the slightly lower synthesis of FT compounds in configuration C.3 with respect to C.2, although both designs recycle 95 % of the off-gas. Finally, configurations C.4 and C.5 present very similar production results in terms of liquid fraction. In case C.4, carbon dioxide is looped only within the RWGS reactor, determining a conversion to CO by reaction with unconverted hydrogen. Contrarywise, in C.5 part of the FT off-gas are sent to the calciner for the oxy-combustion process, determining a rise in the CO_2 content sent to the RWGS and the latter higher demand for hydrogen and a higher throughput of light gases.

In terms of products distribution, configuration C.2 should be discarded, as the shift towards heavy hydrocarbons is not as remarkable as in the other cases. C.1 can be a profitable solution to shift towards high molecular weight products, but it presents a distribution peak at C_7 (the highest carbon number peak among the configurations, as depicted in the zoomed section of Fig. 4) which turns in a tail at carbon number higher than $C_{40\text{-}45}$ going towards C.2. Lastly, configurations C.3, C.4, and C.5 suggest being the most suitable solution when targeting heavy hydrocarbons due to the higher concentration of products with a carbon number higher than C_{20+}. This result is interesting from an economic standpoint, since recent market analyses report demand for heavy waxes in the paraffinic form [80].

As a matter of fact, looping the FT off-gas to the DAC and the RWGS units allow reforming of light hydrocarbons. Moreover, dragging inert nitrogen in the recirculated flows could influence the partial pressures of reactants in both the RWGS and the FT reactors and their efficiencies, shifting the selectivity towards heavier hydrocarbons [4,81]. Remarkably, no solid carbon is deposited onto the RWGS reactor in any of the cases, thus no addition of external oxygen carrier to this reactor is required (See supporting material for C-deposition check).

3.2. Energy balance

The information about energy balances is provided in Table 8. Considering the electric power, the electrolyzer is the most energy-intensive component, accounting for more than 85 % of the absorbed power regardless of the system configurations. Remarkably, C.4 is the configuration with the lowest electrolyzer consumption, possibly due to a more virtuous hydrogen management provided by the FT off-gas recirculation to the RWGS only. Contrarywise, when recycling the FT off-gas to the DAC unit, hydrogen exists the system in the form of water, due to reaction in the calciner reactor. However, configuration C.4 requires 128 MW_{el} to sustain the reactions evolving in the electrified calciner.

Table 8
Energy balance information for each configuration.

[MW]	*C.1*	*C.2*	*C.3*	*C.4*	*C.5*
Electric power					
Auxiliaries	0.92	0.69	0.72	0.63	0.83
CC Compression	22.06	22.35	22.40	0.00	0.00
FT compression	101.05	32.26	43.81	59.09	66.25
Electrolysis	838.09	707.16	784.31	646.74	858.14
CC Turbine	−30.01	−30.00	−30.03	0.00	0.00
Slake Steam-Turbine	−22.39	−24.92	−24.95	−21.88	−25.06
Chemical content					
NG/FT off-gas CC	140.54	0	0.00	0.00	0.00
NG/FT off-gas Calciner	127.55	0	0.00	0.00	0.00
FT liquid products	−419.78	−166.49	−235.84	−337.73	−331.21
Thermal power					
Heaters	343.03	293.80	301.00	334.51	324.75
Coolers	−507.80	−339.40	−339.60	−339.22	−386.63
RWGS reactor	182.12	41.14	69.53	123.67	117.86
FT reactor	−210.36	−80.94	−111.30	−154.80	−159.81
Pellet reactor	−13.14	−6.77	−6.93	−5.47	−5.47
Slaker reactor	−46.31	−41.89	−41.89	−46.31	−41.89
TG Comb	−81.27	−1.97	−11.14	0.00	0.00
Calciner	0.00	0.00	0.00	128.47	0.00

Regarding the chemical power of NG, this directly depends on the mass flow rate entering the combined cycle and the calciner. 64 % of the power content of the NG is fed to the calciner in C.1. Moreover, given the higher amount of FT liquid products obtained in C.1, this configuration also provides the highest energy content in the synthetic hydrocarbons. However, such a thermal power is completely avoided for all the other configuration, where NG is excluded.

With respect to the thermal power of the system, the heaters absorb more than 60 % of the required thermal power, with a peak of 86.2 % required for the heaters in configuration C.2 and 64.3 % as the lowest condition in design C.1. Similarly, coolers in design C.1 require 58.8 % of the cooling power, whereas in C.2 account for 70.9 %, C.3 65.3 %, C.4 61.2 %, C.5 64.1 %. Concerning the main components of the plant, the washer and the absorber column disperse thermal power to the

environment, while calciner operates at adiabatic conditions, besides under configuration C.4. However, heat fluxes exchanged by the flows at inlets and outlets of these components are considered in the heaters and coolers. The RWGS reactor is the most critical component: it requires a high amount of thermal power for isothermal conditions, with C.1 requiring 182 MWth for operations as the highest value, and C.2 requiring 41 MWth as the lowest value (Fig. 5).

3.3. Thermal integration

Thermal integration among cold and hot streams through a network of recovery heat exchangers ($\Delta T_{min} = 15$ °C) was investigated applying pinch analysis methodology to minimize the heat supply from the environment. Fig. 6 provides the results on the pinch analysis applied to the considered system configurations. Both hot and cold composite curves are shown. Table 9 presents the thermal energy required by each case before and after optimal energy integration. It is worth noting how the integration process sensibly reduces the heat required by the plant.

Even in this case, it is possible to address the RWGS reactor as the most critical thermal sink, creating a plateau at 800 °C. In the case of surplus energy demand, electric heaters could supply the required amount. Moreover, in all the cases studied, three plateaux can be identified in the hot composite curves at 300 °C, 230 °C and 99 °C corresponding to the slaker reactor, the FT reactor and the phase change of the steam leaving the slaker steam turbine, respectively. The first two heat fluxes can potentially be employed to heat low-temperature streams (e.g., the steam entering the slaker), and to preheat the gas mixture entering the RWGS reactor

3.4. Key performance indicators

KPIs were evaluated considering each case under the optimal energy integration presented in section 3.3: these are presented in Table 10. Configuration C.1 has the highest energy consumption per mass of CO_2 removed from the air ($E_{SPCO2} = 13.9$ kW h/kg_{CO2}) due to the feeding of extra natural gas. However, it reaches the midd value of 154.7 kW h/kg_{wax} thanks to the highest production of FT material. It also presents a plant efficiency η_{GI} of 31.2 %, a CO_2 removal efficiency η_{CO2} of 64.4 % and a carbon efficiency η_C of 73.8 %. The latter is the highest among the configurations, due to the presence of additional carbon material fed with natural gas.

On the contrary, it is possible to note how solution C.2 provides the highest energy consumption when referred to the amount of FT waxes produced by the system (210.5 kW h/kg_{wax}), as well as the lowest system efficiency and carbon conversion (58.1 % and 22.6 %). Hence, once again, configuration C.2 shall be discarded. It is to note that the carbon conversion and the CO_2 conversion efficiencies of C.2-C.5 are the same, as no additional carbon is fed with the avoidance of fossil natural gas.

Moreover, C.3 η_{GI} and η_C are only a few percentage points lower than the corresponding values of C.1, and it is important to remark that configuration C.3 has the highest value of carbon dioxide removal from the air (almost $\eta_{CO2} = 70$ %). This means that substituting the flow of NG with FT off-gas considerably increases the usage of carbon material captured from the air, and it is beneficial from an environmental point of view, when presenting high FT off-gas recirculation rates. From this point of view, even C.4 and C.5 have better performance than C.1, both as global plant efficiency and conversion of carbon dioxide into FT material. Moreover, configuration C.4 provides the highest η_{GI} at 36.5 %, connected to the much lower electric demand of the electrolyser.

Thus, from a production perspective, configuration design C.1 can be preferential. Nonetheless, configuration C.3 results in a most suitable solution to extract CO_2 from the air, with C.4 and C.5 outperforming C.1 also in terms of plant efficiency.

4. Economic evaluation

The economic analysis provides the systems installation and operations costs, as well as economic indicators identified in the FT wax production cost and the CO_2 removal cost.

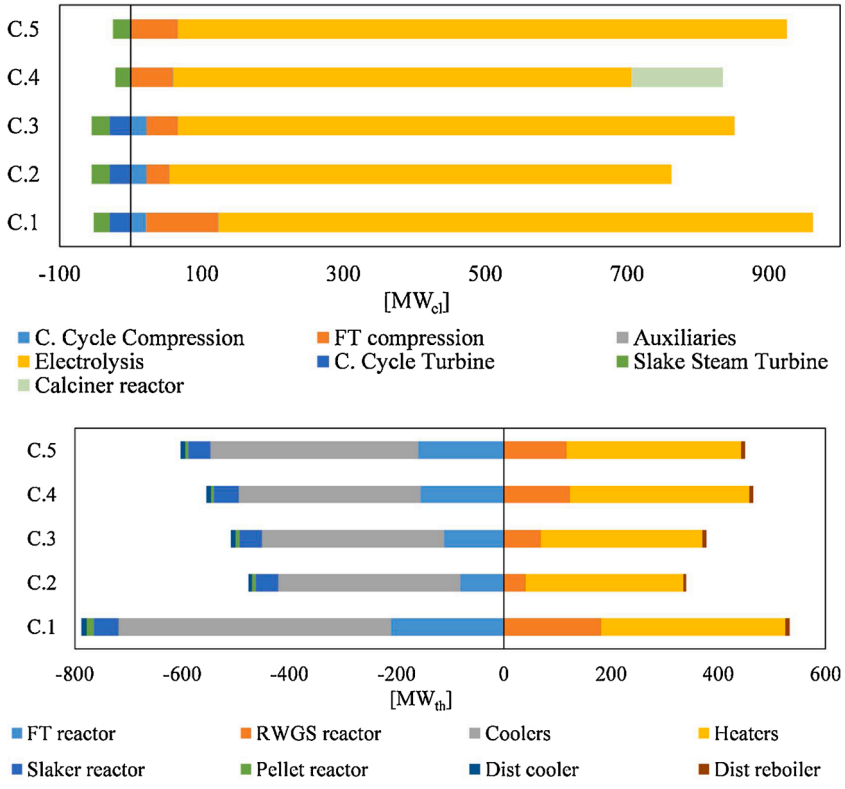

Fig. 5. Inlet and outlet power for the main plant components: electric (top) and thermal powers (bottom) are shown.

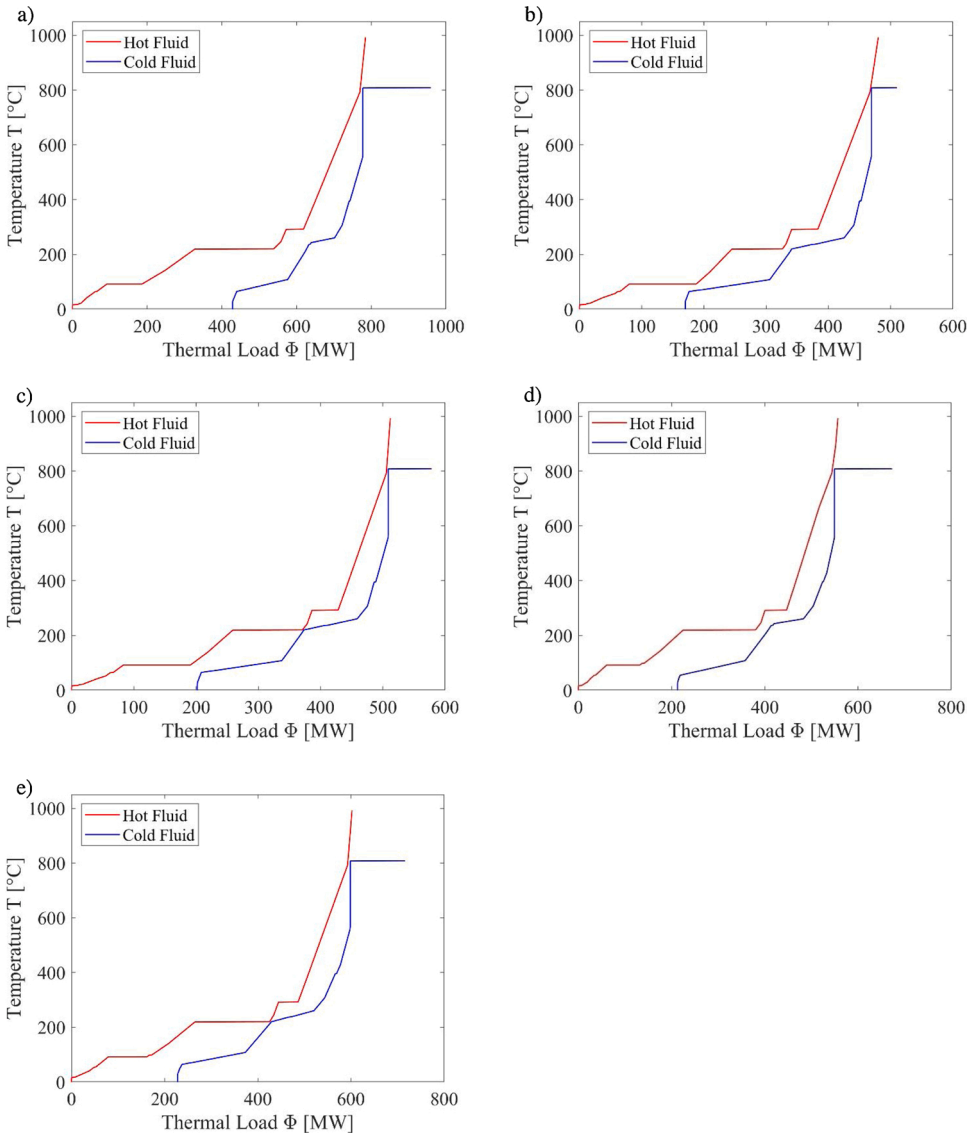

Fig. 6. Hot and cold composite curves for each configuration derived by the Pinch Analysis: a) C.1; b) C.2; c) C.3; d) C.4; e) C.5.

Table 9
Energy integration effect on the plants heat demand.

[MW_{th}]	*C.1*	*C.2*	*C.3*	*C.4*	*C.5*
Heat Demand W/o Integration	531.0	342.8	379.0	592.4	487.9
Heat Demand W/ Integration	168.2	28.8	63.7	111.8	109.1

Table 10
Key performance indicators results.

KPI	*C.1*	*C.2*	*C.3*	*C.4*	*C.5*
E_{SPco2} [kWh/kg_{CO2}]	13.9	8.5	8.4	9.2	10.1
E_{SPwax} [kWh/kg_{wax}]	154.7	210.5	179.2	133.4	147.8
η_C	73.78 %	58.1 %	68.3 %	67.2 %	66.4 %
η_{CO2}	64.4 %	58.1 %	68.3 %	67.2 %	66.4 %
η_{GI}	31.2 %	22.6 %	27.2 %	36.5 %	32.8 %

4.1. Capital cost

Following the methodology described in Section 2.5, an overall CAPEX of 1.87 G€ (billions of €) was obtained for the baseline scenario C.1. From Fig. 7 it is possible to note a reduction of the CAPEX value of

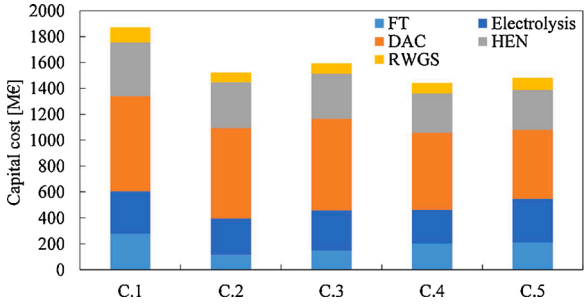

Fig. 7. Distribution of the CAPEX in the different sections of the CCU plant.

14–23 % in scenarios C.2 to C.5. Specifically, this is mainly related to a lower cost of the RWGS and the FT reactors units, where a higher amount of material processed in C.1 determine a rise in their capital costs. Additionally, for configurations C.4 and C.5, the reduced value is connected to the lower installation costs applied for the DAC section, either electrified or without the combined cycle section [9], and the reduced size of the electrolyser of C.4. In all the studied configurations, the DAC unit accounts between 28.6 % (in C.5) to 39.2 % (in C.2) of the

total CAPEX, the electrolyser between 14%–18%, while the FT synthesis unit and distillation unit account for 6–15 % of the CAPEX. A detailed cost breakdown is provided in Table S5 of the Supporting Material.

4.2. Operating costs

With a comprehensive estimation of the operating costs starting from the mass and energy balances of the plant, the breakdown of the OPEX is provided in Fig. 8, with a presentation of both non-electric and electric OPEX. In all the studied configurations, the sum of the non-electric OPEX ranges between 89 and 129 M€/y, corresponding to C.4 and C.1, respectively. The non-electric OPEX value is counterbalanced by the revenues from the sale of the process by-products: oxygen, naphtha, and middle FT distillate. Specifically for configurations C.1, C.4, and C.5, the revenues exceed the non-electric OPEX (149 vs. 129 M€/y, 135 vs. 89 M€/y, and 134 vs. 100 M€/y, respectively), with a beneficial effect on the plant economics. In configuration C.3, the same value of revenues and non-electric OPEX is reached (103.2 and 104 M€/y, respectively), while C.2 has non-beneficial costs, with the non-electric OPEX being at 102 M€/y and revenues at only 81 M€/y.

Moreover, the cost of running the electrically fed equipment of the plants was studied (i.e., electric OPEX). The biggest contribution to the electric operating costs is represented by the electrolysis section, in compliance with the outcome of the energy balance (Table 8). Depending on the plant configuration, this cost represents between 70–78 % of the electric OPEX in the scenario fed with hydropower-generated electricity, and up to 79–90 % in in the scenario employing CSP electricity. Lastly, the overall highest electric OPEX was found in the process design C.1. As expected, based on the costs selected, the hydropower is the most effective solution, reaching the lowest values of electric-related OPEX. However, as mentioned in the Methodology section, the cost of electricity based on baseload values from mix RES provides a more conservative value [69].

4.3. Production costs

Fig. 9 depicts the costs of FT waxes production evaluated according to eq. (8). Configuration C.1 and C.4 reach similar wax production costs, with this C.4 being the most promising configuration. In this case, the wax production cost ranges between 5.05 €/kg_{wax} and 25.0 €/kg_{wax} at 0% interest rate, 6.3 €/kg_{wax} and 26.3 €/kg_{wax} at 7.5 %, and 7.4 €/kg_{wax} and 27.4 €/kg_{wax} at 12.5 %, where the lower costs result from hydropower electricity feed and the higher costs from mixed RES baseload electricity feed. In the case of C.1, its low production cost can be related to the high amount of Fischer-Tropsch material that is produced. On the contrary, for C.4, such a cost is related to the low installation cost and operating costs. Moreover, even from a cost of wax production point of view, configuration C.2 shall be discarded as preferential one, given the high installation costs and low throughput of FT compounds. Finally, configuration C.3 and C.5 are the intermediate solutions, with C.5 reaching a lower production costs given the avoidance of the combined cycle unit. For this configuration, the cost range corresponds to 6.7–32.3 €/kg_{wax} at 0% interest rate, 8.0–33.7 €/kg_{wax} at 7.5 %, and 9.2–34.8 €/kg_{wax} at 12.5 %.

Fig. 9. Ranges of the cost of FT waxes production under different interest rates. The minimum price level corresponds to hydropower electricity source, the maximum to baseload one.

From an FT production cost point of view, the present system results in a higher marginal value compared to market fossil-derived paraffin wax cost that is about 2.50 €/kg_{wax}, even when considering low-priced electricity scenarios [82,83]. This can be related to the electrolyser and DAC units cost, which may be economically unfeasible without carbon credits or incentives. For instance, Karki et al. [84] determined a cost of 2.40 €/kg_{wax} (carbon number C_{18+}) when exploiting the CO_2 from a concentrated point source, making the source of CO_2 economically relevant. Hence, external incentives would be required for the feasible production of synthetic material with this type of route. As stated by Herz et al. [83], a CO_2 compensation of 300 €/t_{CO2} might allow the market entry of alternative-to-oil routes for hydrocarbons production. Considering the upper-cost reference of 2.50 €/kg_{wax}, the present system would reach a feasible solution under configuration C.1, C.4, and C.5 at interest rates of 0% (compensation of 204 €/t_{CO2}, 175 €/t_{CO2}, and 287 €/t_{CO2}, respectively) and configuration C.1 and C.4 at interest rate of 7.5 % (compensation of 282 €/t_{CO2} and 264 €/t_{CO2}) in scenario of electricity supply from hydropower source. If onshore wind electricity was to be employed, the feasibility would be granted only at 0% interest rate for configurations C.1 and C.4, with a carbon dioxide compensation of 282 €/t_{CO2} and 264 €/t_{CO2}, respectively. Contrarywise, for C.4 (the most promising configuration) if baseload electricity was utilized, a credit 1549 €/t_{CO2} would be needed.

4.4. Future production cost

Utilizing baseload electricity of mixed source is currently unfeasible,

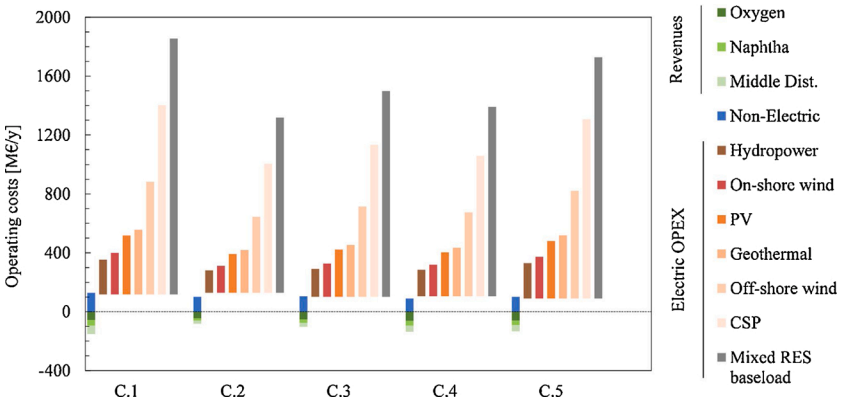

Fig. 8. Revenues and operating costs considered in the definition of the free cash flow.

from both a waxes production cost point of view and a possible compensation related to the amount of carbon dioxide removed from the air. Hence, in accordance with the forecast analyses proposed by Fasihi et al. [9,69] and Gorre et al. [76], the costs of FT waxes production in the year 2030 and 2050 are provided in Fig. 10. Predictably, both the application of experience rates on the cost of components and a reduction of the baseload electricity cost provide a sensible reduction in the year 2030 and 2050 compared to the baseline analysis. Predictably, configuration C.4 remains the most profitable solution: at year 2030 the wax production cost ranges from 7.9 €/t_{CO2} to 9.0 €/t_{CO2}, and 5.9 and 6.7 €/t_{CO2} at the year 2050 (Table 11). Such a cost could be further reduced if the actual learning rates of the DAC and electrolyser technologies would increase up to 20%.

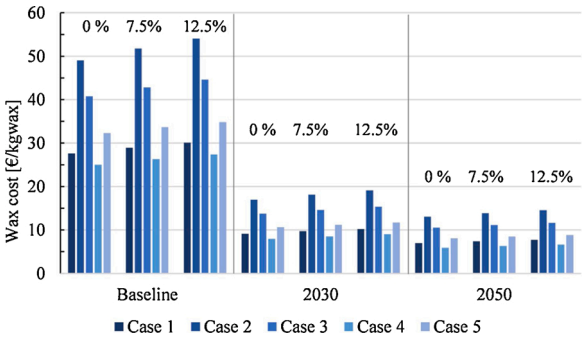

Fig. 10. Cost of wax production utilizing baseload electricity in the year 2030 and 2050.

Table 11
Evolution of CAPEX and OPEX at the year 2030 and 2050. [a]Accounted at the baseload electricity price.

CAPEX	*Unit*	*C.1*	*C.2*	*C.3*	*C.4*	*C.5*
Baseline	M€	1871	1524	1595	1440	1483
2030	M€	796	653	667	655	639
2050	M€	575	449	463	458	454
OPEX[a]						
Baseline	M€/y	1996.3	1393.6	1604.9	1465.6	1839.8
2030	M€/y	754.9	529.5	604.5	550.7	688.8
2050	M€/y	612.7	429.0	489.0	444.4	557.0
Revenues	M€/y	149.9	81.0	103.2	135.2	133.7

5. Conclusions

In the baseline configuration, 124 t/h of CO_2 are utilized to synthesize 8.7 t/h of Fischer-Tropsch waxes, with a plant efficiency (η_{GI}) of 33.2 %. In configurations C.2, C.3, C.4 and C.5, the net FT waxes production corresponds to 3.5 t/h, 4.8 t/h, 6.9 t/h and 6.8 t/h, respectively. Consequently, the plant efficiency changes to 22.6 %, 27.2 %, 36.5 %, and 32.8 %, respectively, due to the variation in both the FT production and energy consumption. Lastly, η_{CO2} varies to 58.1 %, 68.3 %, 67.2 %, and 66.4 % in C.2, C.3, C.4, and C.5 configurations, respectively, starting from the baseline value of 31.2 % (configuration C.1). Hence, considering only the production of FT material, configuration C.1 is the most effective solution. However, this configuration comes with the drawback of utilizing natural gas, a fossil material that has to be avoided. Hence, this configuration should be avoided. From an environmental point of view, configuration C.3 is the most effective in removing carbon dioxide from the air, only one percentage point higher than in configuration C.4. Finally, configuration C.4 is the best one when considering the overall production costs of FT waxes. If utilizing hydropower electricity source, this cost corresponds to 5.05 €/kg_{wax}. Carbon credits can provide a feasible market entry of this CO_2-to-FT wax route, that helps offsetting the high capital cost of the DAC unit. At 7.5 % interest rate for the scenario C.4, the FT wax breakeven can be reached at 264 €/t_{CO2} with electricity from hydropower source. At 0% interest rate, the same result is reached with 175 €/kg_{CO2} as credits. Moreover, if utilizing baseload electricity, profitable applications of this process route shall be expected from the year 2030, when a reduction of the components cost (DAC, electrolyser, system reactors) and of the baseload electricity cost from mixed RES can be expected.

Funding

This work received funding from the Politecnico di Torino and the European Union's *Horizon 2020 research and innovation programme* under grant agreement No. 768543 ("ICO2CHEM").

CRediT authorship contribution statement

Marco Marchese: Conceptualization, Methodology, Formal analysis, Investigation, Software, Data curation, Writing - original draft, Visualization. **Giulio Buffo:** Conceptualization, Investigation, Data curation, Writing - review & editing. **Massimo Santarelli:** Supervision, Writing - review & editing. **Andrea Lanzini:** Supervision, Project administration, Writing - review & editing.

Declaration of Competing Interest

N.A.

Appendix A. Supplementary data

Supplementary data associated with this article can be found, in the online version, at https://doi.org/10.1016/j.jcou.2021.101487.

References

[1] Global Warming of 1.5 °C - An IPCC Special Report on the Impacts of Global Warming of 1.5°C Above pre-Industrial Levels and Related Global Greenhouse Gas Emission Pathways, in the Context of Strengthening the Global Response to the Threat of Climate Chang, IPCC, Geneva, Switzerland, 2018.
[2] European Commission, A Clean Planet for All - A European Long-Term Strategic Vision for a Prosperous, Modern, Competitive and Climate Neutral Economy, Eur. Comm., 2018, p. 114. https://ec.europa.eu/clima/sites/clima/files/docs/pages/com_2018_733_en.pdf?utm_campaign=AktuellHållbarhet-Direkten_181129_Username&utm_medium=email&utm_source=Eloqua&elqTrackId.
[3] E. Rozzi, F.D. Minuto, A. Lanzini, P. Leone, Green synthetic fuels: renewable routes for the conversion of non-fossil feedstocks into gaseous fuels and their end uses, Energies 13 (2020), https://doi.org/10.3390/en13020420.
[4] G. Herz, E. Reichelt, M. Jahn, Techno-economic analysis of a co-electrolysis-based synthesis process for the production of hydrocarbons, Appl. Energy 215 (2018) 309–320, https://doi.org/10.1016/j.apenergy.2018.02.007.
[5] G. Buffo, D. Ferrero, M. Santarelli, A. Lanzini, Energy and environmental analysis of a flexible power-to-X plant based on reversible solid oxide cells (rSOCs) for an urban district, J. Energy Storage 29 (2020) 101314, https://doi.org/10.1016/j.est.2020.101314.
[6] J. Lehtonen, V. Järnefelt, S. Alakurtti, A. Arasto, I. Hannula, A. Harlin, T. Koljonen, R. Lantto, M. Lienemann, K. Onarheim, J.-P. Pitkänen, M. Tähtinen, The carbon reuse economy: transforming CO_2 from a pollutant into a resource, VTT Tech. Res. Cent. Finl. (2019), https://doi.org/10.32040/2019.978-951-38-8709-4.
[7] D.W. Keith, Why capture CO_2 from the atmosphere? Science (80-.) 325 (2009) 1654–1655, https://doi.org/10.1126/science.1175680.
[8] F.D. Meylan, V. Moreau, S. Erkman, CO_2 Utilization in the Perspective of Industrial Ecology, an Overview, 2015, https://doi.org/10.1016/j.jcou.2015.05.003.
[9] M. Fasihi, O. Efimova, C. Breyer, Techno-economic assessment of CO_2 direct air capture plants, J. Clean. Prod. 224 (2019) 957–980, https://doi.org/10.1016/j.jclepro.2019.03.086.
[10] E.S. Sanz-Pérez, C.R. Murdock, S.A. Didas, C.W. Jones, Direct capture of CO_2 from ambient air, Chem. Rev. 116 (2016) 11840–11876, https://doi.org/10.1021/acs.chemrev.6b00173.
[11] F. Zeman, Energy and material balance of CO_2 capture from ambient air, Environ. Sci. Technol. 41 (2007) 7558–7563, https://doi.org/10.1021/es070874m.
[12] V. Nikulshina, C. Gebald, A. Steinfeld, CO_2 capture from atmospheric air via consecutive CaO-carbonation and $CaCO_3$-calcination cycles in a fluidized-bed solar reactor, Chem. Eng. J. (2009), https://doi.org/10.1016/j.cej.2008.06.005.
[13] R.M. Cuéllar-Franca, A. Azapagic, Carbon capture, storage and utilisation technologies: a critical analysis and comparison of their life cycle environmental impacts, J. CO2 Util. 9 (2015) 82–102, https://doi.org/10.1016/j.jcou.2014.12.001.

[14] S.M. Jarvis, S. Samsatli, Technologies and infrastructures underpinning future CO_2 value chains: a comprehensive review and comparative analysis, Renew. Sustain. Energy Rev. 85 (2018) 46–68, https://doi.org/10.1016/j.rser.2018.01.007.

[15] N. Moazami, M.L. Wyszynski, K. Rahbar, A. Tsolakis, H. Mahmoudi, A comprehensive study of kinetics mechanism of Fischer-Tropsch synthesis over cobalt-based catalyst, Chem. Eng. Sci. 171 (2017) 32–60, https://doi.org/10.1016/j.ces.2017.05.022.

[16] E. Iglesia, Design, synthesis, and use of cobalt-based Fischer-Tropsch synthesis catalysts, Appl. Catal. A, Gen. 161 (1997) 59–78.

[17] A. Rafiee, M. Panahi, K.R. Khalilpour, CO_2 utilization through integration of post-combustion carbon capture process with Fischer-Tropsch gas-to-liquid (GTL) processes, J. CO_2 Util. 18 (2017) 98–106, https://doi.org/10.1016/j.jcou.2017.01.016.

[18] S.S. Ail, S. Dasappa, Investigations into enhanced wax production with combustion synthesized Fischer-Tropsch catalysts, Energy Convers. Manag. 116 (2016) 80–90, https://doi.org/10.1016/j.enconman.2016.02.075.

[19] F. Vidal Vázquez, J. Koponen, V. Ruuskanen, C. Bajamundi, A. Kosonen, P. Simell, J. Ahola, C. Frilund, J. Elfving, M. Reinikainen, N. Heikkinen, J. Kauppinen, P. Piermartini, Power-to-X technology using renewable electricity and carbon dioxide from ambient air: SOLETAIR proof-of-concept and improved process concept, J. CO_2 Util. 28 (2018) 235–246, https://doi.org/10.1016/j.jcou.2018.09.026.

[20] Kopernikus projekte, 2019. https://www.kopernikus-projekte.de/.

[21] P. Viebahn, A. Scholz, O. Zelt, The potential role of direct air capture in the German energy research program—results of a multi-dimensional analysis, Energies 12 (2019) 1–27, https://doi.org/10.3390/en12183443.

[22] C. van der Giesen, R. Kleijn, G.J. Kramer, Energy and climate impacts of producing synthetic hydrocarbon fuels from CO $_2$, Environ. Sci. Technol. 48 (2014) 7111–7121, https://doi.org/10.1021/es500191g.

[23] M. Fasihi, D. Bogdanov, C. Breyer, Economics of Global Gas-To-Liquids (GtL) Fuels Trading Based on Hybrid Pv-Wind Power Plants; Economics of Global Gas-To-Liquids (GtL) Fuels Trading Based on Hybrid Pv-Wind Power Plants, 2015.

[24] M. Fasihi, D. Bogdanov, C. Breyer, Techno-economic assessment of power-to-liquids (PtL) fuels production and global trading based on hybrid PV-wind power plants, Energy Procedia (2016) 243–268, https://doi.org/10.1016/j.egypro.2016.10.115. Elsevier Ltd.

[25] M. Fasihi, D. Bogdanov, C. Breyer, Long-term hydrocarbon trade options for the Maghreb region and Europe-renewable energy based synthetic fuels for a net zero emissions world, Sustain 9 (2017), https://doi.org/10.3390/su9020306.

[26] C.M. Liu, N.K. Sandhu, S.T. Mccoy, J.A. Bergerson, A Life Cycle Assessment of Greenhouse Gas Emissions from Direct Air Capture and Fischer-Tropsch Fuel Production, 2020, https://doi.org/10.1039/c9se00479c.

[27] M. Mansouri, H. Atashi, A.A. Mirzaei, Hydrogenation of CO on cobalt catalyst in Fischer–Tropsch synthesis, J. Thermodyn. Catal. 03 (2012), https://doi.org/10.4172/2157-7544.1000113.

[28] D.W. Keith, G. Holmes, D.St. Angelo, K. Heidel, A process for capturing CO2 from the atmosphere, Joule 2 (2018) 1573–1594, https://doi.org/10.1016/j.joule.2018.05.006.

[29] S. Jürgens, P. Oßwald, M. Selinsek, P. Piermartini, J. Schwab, P. Pfeifer, U. Bauder, S. Ruoff, B. Rauch, M. Köhler, Assessment of combustion properties of non-hydroprocessed Fischer-Tropsch fuels for aviation, Fuel Process. Technol. 193 (2019) 232–243, https://doi.org/10.1016/j.fuproc.2019.05.015.

[30] K.S. Lackner, Capture of carbon dioxide from ambient air, Eur. Phys. J. Spec. Top. 176 (2009) 93–106, https://doi.org/10.1140/epjst/e2009-01150-3.

[31] C. Falter, V. Batteiger, A. Sizmann, Climate Impact and Economic Feasibility of Solar Thermochemical Jet Fuel Production, 2015, https://doi.org/10.1021/acs.est.5b03515.

[32] L.E. Hombach, L. Doré, K. Heidgen, H. Maas, T.J. Wallington, G. Walther, Economic and environmental assessment of current (2015) and future (2030) use of E-fuels in light-duty vehicles in Germany, J. Clean. Prod. 207 (2019) 153–162, https://doi.org/10.1016/j.jclepro.2018.09.261.

[33] A. García, J. Monsalve-Serrano, D. Villalta, R.L. Sari, V. Gordillo Zavaleta, P. Gaillard, Potential of e-Fischer Tropsch Diesel and Oxymethyl-Ether (OMEx) as Fuels for the Dual-Mode Dual-Fuel Concept, 2019, https://doi.org/10.1016/j.apenergy.2019.113622.

[34] P. Schmidt, V. Batteiger, A. Roth, W. Weindorf, T. Raksha, Power-to-liquids as renewable fuel option for aviation: a review, Chemie-Ingenieur-Technik 90 (2018) 127–140, https://doi.org/10.1002/cite.201700129.

[35] P. Schmidt, W. Weindorf, Power-to-Liquids: Potentials and Perspectives for the Future Supply of Renewable Aviation Fuel, 2016. https://www.umweltbundesamt.de/en/publikationen/power-to-liquids-potential-perspectives-for-the.

[36] C. Panzone, R. Philippe, A. Chappaz, P. Fongarland, A. Bengaouer, Power-to-liquid catalytic CO_2 valorization into fuels and chemicals: focus on the Fischer-Tropsch route, J. CO2 Util. 38 (2020) 314–347, https://doi.org/10.1016/j.jcou.2020.02.009.

[37] C. Graves, S.D. Ebbesen, M. Mogensen, K.S. Lackner, Sustainable hydrocarbon fuels by recycling CO2 and H 2O with renewable or nuclear energy, Renew. Sustain. Energy Rev. 15 (2011) 1–23, https://doi.org/10.1016/j.rser.2010.07.014.

[38] S. Horvath, M. Fasihi, C. Breyer, Techno-economic analysis of a decarbonized shipping sector: technology suggestions for a fleet in 2030 and 2040, Energy Convers. Manag. 164 (2018) 230–241, https://doi.org/10.1016/j.enconman.2018.02.098.

[39] Agora Verkehrswende, Agora Energiewende and Frontiers Economics: The Future Cost of Electricity-Based Synthetic Fuels, 2018 (accessed January 29, 2021), www.agora-verkehrswende.de.

[40] C. Beuttler, L. Charles, J. Wurzbacher, The role of direct air capture in mitigation of anthropogenic greenhouse gas emissions, Front. Clim. 1 (2019) 10, https://doi.org/10.3389/fclim.2019.00010.

[41] M. Loewert, M. Riedinger, P. Pfeifer, Dynamically operated Fischer–Tropsch synthesis in PtL—Part 2: coping with Real PV profiles, Chem. Eng. 4 (2020) 27, https://doi.org/10.3390/chemengineering4020027.

[42] M. Loewert, P. Pfeifer, Dynamically operated Fischer-Tropsch synthesis in PtL-part 1: system response on intermittent feed, Chem. Eng. 4 (2020) 21, https://doi.org/10.3390/chemengineering4020021.

[43] S. Drünert, U. Neuling, T. Zitscher, M. Kaltschmitt, Power-to-liquid fuels for aviation – processes, resources and supply potential under German conditions, Appl. Energy 277 (2020) 115578, https://doi.org/10.1016/j.apenergy.2020.115578.

[44] V. Dieterich, A. Buttler, A. Hanel, H. Spliethoff, S. Fendt, Power-to-liquid via synthesis of methanol, DME or Fischer–Tropsch-fuels: a review, Energy Environ. Sci. 13 (2020) 3207–3252, https://doi.org/10.1039/d0ee01187h.

[45] H. Blanco, W. Nijs, J. Ruf, A. Faaij, Potential for hydrogen and power-to-liquid in a low-carbon EU energy system using cost optimization, Appl. Energy 232 (2018) 617–639, https://doi.org/10.1016/j.apenergy.2018.09.216.

[46] R. Baciocchi, G. Storti, M. Mazzotti, Process design and energy requirements for the capture of carbon dioxide from air, Chem. Eng. Process. 45 (2006), https://doi.org/10.1016/j.cep.2006.03.015.

[47] W.K. Lewis, W.G. Whitman, Principles of gas absorption, Ind. Eng. Chem. 16 (1924) 1215–1220, https://doi.org/10.1021/ie50180a002.

[48] S. Moioli, L.A. Pellegrini, S. Gamba, Simulation of CO_2 capture by MEA scrubbing with a rate-based model, Procedia Eng. 42 (2012) 1651–1661, https://doi.org/10.1016/j.proeng.2012.07.558.

[49] Tractebel, Engie, Hinicio, Study on Early Business Cases for H_2 in Energy Storage and More Broadly Power To H_2 Applications, 2017 https://doi.org/fch.europa.eu/sites/default/files/P2H_Full_Study_FCHJU.pdf.

[50] F. Vidal Vázquez, P. Pfeifer, J. Lehtonen, P. Piermartini, P. Simell, V. Alopaeus, Catalyst screening and kinetic modeling for CO production by High pressure and temperature reverse Water gas shift for Fischer-Tropsch applications, Ind. Eng. Chem. Res. 56 (2017) 13262–13272, https://doi.org/10.1021/acs.iecr.7b01606.

[51] M. Marchese, N. Heikkinen, E. Giglio, A. Lanzini, J. Lehtonen, M. Reinikainen, Kinetic study based on the carbide mechanism of a Co-Pt/γ-Al_2O_3 Fischer–Tropsch catalyst tested in a laboratory-scale tubular reactor, Catalysts 9 (2019) 717, https://doi.org/10.3390/catal9090717.

[52] M. Marchese, E. Giglio, M. Santarelli, A. Lanzini, Energy performance of power-to-liquid applications integrating biogas upgrading, reverse water gas shift, solid oxide electrolysis and Fischer-Tropsch technologies, Energy Convers. Manag. X (2020) 100041, https://doi.org/10.1016/j.ecmx.2020.100041.

[53] F.J. Campanario, F.J. Gutiérrez Ortiz, Fischer-Tropsch biofuels production from syngas obtained by supercritical water reforming of the bio-oil aqueous phase, Energy Convers. Manag. 150 (2017) 599–613, https://doi.org/10.1016/j.enconman.2017.08.053.

[54] P.M. Maitlis, A. de Klerk, Greener Fischer-Tropsch Processes for Fuels and Feedstocks, 2013, https://doi.org/10.1002/9783527656837.

[55] Chemical Engineering, 2019 Chemical Engineering Plant Cost Index Annual Average, 2020.

[56] D.W. Keith, G. Holmes, D.St. Angelo, K. Heidel, A process for capturing CO2 from the atmosphere, Joule 2 (2018) 1573–1594, https://doi.org/10.1016/j.joule.2018.05.006.

[57] G. Herz, E. Reichelt, M. Jahn, Design and evaluation of a Fischer-Tropsch process for the production of waxes from biogas, Energy 132 (2017) 370–381, https://doi.org/10.1016/j.energy.2017.05.102.

[58] K. Atsonios, K.D. Panopoulos, E. Kakaras, Investigation of technical and economic aspects for methanol production through CO_2, Int. J. Hydrogen Energy 41 (2016) 2202–2214, https://doi.org/10.1016/j.ijhydene.2015.12.074.

[59] J. Proost, State-of-the art CAPEX data for water electrolysers, and their impact on renewable hydrogen price settings, Int. J. Hydrogen Energy 44 (2019) 4406–4413, https://doi.org/10.1016/j.ijhydene.2018.07.164.

[60] R.U. Dietrich, F.G. Albrecht, S. Maier, D.H. König, S. Estelmann, S. Adelung, Z. Bealu, A. Seitz, Cost calculations for three different approaches of biofuel production using biomass, electricity and CO_2, Biomass Bioenergy 111 (2018) 165–173, https://doi.org/10.1016/j.biombioe.2017.07.006.

[61] W.L. Becker, R.J. Braun, M. Penev, M. Melaina, Production of Fischer-Tropsch liquid fuels from high temperature solid oxide co-electrolysis units, Energy 47 (2012) 99–115, https://doi.org/10.1016/j.energy.2012.08.047.

[62] L.J.F. Comidy, M.D. Staples, S.R.H. Barrett, Technical, economic, and environmental assessment of liquid fuel production on aircraft carriers, Appl. Energy 256 (2019) 113810, https://doi.org/10.1016/j.apenergy.2019.113810.

[63] M. Decker, F. Schorn, R.C. Samsun, R. Peters, D. Stolten, Off-grid power-to-fuel systems for a market launch scenario – a techno-economic assessment, Appl. Energy 250 (2019) 1099–1109, https://doi.org/10.1016/j.apenergy.2019.05.085.

[64] F.J. Campanario, F.J. Gutiérrez Ortiz, Techno-economic assessment of bio-oil aqueous phase-to-liquids via Fischer-Tropsch synthesis and based on supercritical water reforming, Energy Convers. Manag. 154 (2017) 591–602, https://doi.org/10.1016/j.enconman.2017.10.096.

[65] T.E. Akinola, E. Oko, M. Wang, Study of CO_2 removal in natural gas process using mixture of ionic liquid and MEA through process simulation, Fuel 236 (2019) 135–146, https://doi.org/10.1016/j.fuel.2018.08.152.

[66] M.F. Shehzad, M.B. Abdelghany, D. Liuzza, V. Mariani, L. Glielmo, Mixed logic dynamic models for MPC control of wind farm hydrogen-based storage systems, Inventions 4 (2019) 57, https://doi.org/10.3390/inventions4040057.

[67] M. Hillestad, M. Ostadi, G.d. Alamo Serrano, E. Rytter, B. Austbø, J.G. Pharoah, O. S. Burheim, Improving carbon efficiency and profitability of the biomass to liquid process with hydrogen from renewable power, Fuel 234 (2018) 1431–1451, https://doi.org/10.1016/j.fuel.2018.08.004.
[68] IRENA, Renewable Power Generation Costs in 2019: Latest Trends and Drivers, 2019.
[69] M. Fasihi, C. Breyer, Baseload electricity and hydrogen supply based on hybrid PV-wind power plants, J. Clean. Prod. 243 (2020) 118466, https://doi.org/10.1016/j.jclepro.2019.118466.
[70] L. De Souza Noel Simas Barbosa, J.F. Orozco, D. Bogdanov, P. Vainikka, C. Breyer, Hydropower and power-to-gas storage options: the Brazilian energy system case, Energy Procedia (2016) 89–107, https://doi.org/10.1016/j.egypro.2016.10.101. Elsevier Ltd.
[71] V. Dieterich, A. Buttler, A. Hanel, H. Spliethoff, S. Fendt, Power-to-liquid: via synthesis of methanol, DME or Fischer-Tropsch-fuels: a review, Energy Environ. Sci. 13 (2020) 3207–3252, https://doi.org/10.1039/d0ee01187h.
[72] H2 energy to generate green hydrogen from hydropower in aarau, Fuel Cells Bull. 2016 (2016) 8, https://doi.org/10.1016/s1464-2859(16)30181-x.
[73] A. Hassan, M.K. Patel, D. Parra, An assessment of the impacts of renewable and conventional electricity supply on the cost and value of power-to-gas, Int. J. Hydrogen Energy. (2018), https://doi.org/10.1016/j.ijhydene.2018.10.026.
[74] D. Parigi, E. Giglio, A. Soto, M. Santarelli, Power-to-fuels through carbon dioxide Re-utilization and high-temperature electrolysis: a technical and economical comparison between synthetic methanol and methane, J. Clean. Prod. 226 (2019) 679–691, https://doi.org/10.1016/j.jclepro.2019.04.087.
[75] Cost Estimation Methodology for NETL Assessments of Power Plant Performance DOE/NETL-2011/1455, National Energy Technology Laboratory (NETL), 2019.
[76] J. Gorre, F. Ortloff, C. Van Leeuwen, Production Costs for Synthetic Methane in 2030 and 2050 of an Optimized Power-to-Gas Plant With Intermediate Hydrogen Storage, 2019, https://doi.org/10.1016/j.apenergy.2019.113594.
[77] F.G. Albrecht, D.H. König, N. Baucks, R.U. Dietrich, A standardized methodology for the techno-economic evaluation of alternative fuels – a case study, Fuel 194 (2017) 511–526, https://doi.org/10.1016/j.fuel.2016.12.003.
[78] S. Martin, F.G. Albrecht, P. Van Der Veer, D. Lieftink, R.U. Dietrich, Evaluation of on-site hydrogen generation via steam reforming of biodiesel: process optimization and heat integration, Int. J. Hydrogen Energy (2016) 6640–6652, https://doi.org/10.1016/j.ijhydene.2016.02.138. Elsevier Ltd.
[79] T. Bhatelia, E. Li, Y. Sun, P. Hazewinkel, N. Burke, V. Sage, Chain length dependent olefin re-adsorption model for Fischer-Tropsch synthesis over Co-Al_2O_3 catalyst, Fuel Process. Technol. (2014) 277–289, https://doi.org/10.1016/j.fuproc.2014.03.028.
[80] K.L. Jensen, R.J. Menard, B.C. English, Market Analysis for Fischer-Tropsch Waxes, 2013 https://doi.org/www.se-ibss.org.
[81] A. Chiodini, L. Bua, L. Carnelli, R. Zwart, B. Vreugdenhil, M. Vocciante, Enhancements in biomass-to-liquid processes: gasification aiming at high hydrogen/carbon monoxide ratios for direct Fischer-Tropsch synthesis applications, Biomass Bioenergy 106 (2017) 104–114, https://doi.org/10.1016/j.biombioe.2017.08.022.
[82] 1Grand View Research, Global Paraffin Wax Market, 2019.
[83] G. Herz, E. Reichelt, M. Jahn, Techno-economic analysis of a co-electrolysis-based synthesis process for the production of hydrocarbons, Appl. Energy 215 (2018) 309–320, https://doi.org/10.1016/j.apenergy.2018.02.007.
[84] J. Kärki, T. Thomasson, K. Melin, M. Suomalainen, H. Saastamoinen, M. Hurskainen, S. Mäkikouri, New business opportunities based on biogenic carbon dioxide utilization, 14th Greenh. Gas Control Technol. Conf. Melb. (2018).